

Article

Relationship between Amyloid- β Deposition and the Coupling between Structural and Functional Brain Networks in Patients with Mild Cognitive Impairment and Alzheimer's Disease

Hui Zhang ^{1,2} , Edward S. Hui ^{3,*} , Peng Cao ¹ and Henry K. F. Mak ^{1,2,4,*} 

¹ Department of Diagnostic Radiology, The University of Hong Kong, Hong Kong 999077, China; shirlzh7@hku.hk (H.Z.); caopeng1@hku.hk (P.C.)

² Alzheimer's Disease Research Network, The University of Hong Kong, Hong Kong 999077, China

³ Department of Rehabilitation Sciences, The Hong Kong Polytechnic University, Hong Kong 999077, China

⁴ State Key Laboratory of Brain and Cognitive Sciences, The University of Hong Kong, Hong Kong 999077, China

* Correspondence: edward.s.hui@gmail.com (E.S.H.); makkf@hku.hk (H.K.F.M.); Tel.: +852-2766-6748 (E.S.H.); +852-2255-3307 (H.K.F.M.)

Abstract: Previous studies have demonstrated that the accumulation of amyloid- β ($A\beta$) pathologies has distinctive stage-specific effects on the structural and functional brain networks along the Alzheimer's disease (AD) continuum. A more comprehensive account of both types of brain network may provide a better characterization of the stage-specific effects of $A\beta$ pathologies. A potential candidate for this joint characterization is the coupling between the structural and functional brain networks (SC-FC coupling). We therefore investigated the effect of $A\beta$ accumulation on global SC-FC coupling in patients with mild cognitive impairment (MCI), AD, and healthy controls. Patients with MCI were dichotomized according to their level of $A\beta$ pathology seen in ¹⁸F-flutemetamol PET-CT scans—namely, $A\beta$ -negative and $A\beta$ -positive. Our results show that there was no difference in global SC-FC coupling between different cohorts. During the prodromal AD stage, there was a significant negative correlation between the level of $A\beta$ pathology and the global SC-FC coupling of MCI patients with positive $A\beta$, but no significant correlation for MCI patients with negative $A\beta$. During the AD dementia stage, the correlation between $A\beta$ pathology and global SC-FC coupling in patients with AD was positive. Our results suggest that $A\beta$ pathology has distinctive stage-specific effects on global coupling between the structural and functional brain networks along the AD continuum.

Keywords: amyloid- β deposition; Alzheimer's disease; coupling between functional and structural networks; ¹⁸F-flutemetamol PET-CT; resting-state functional magnetic resonance imaging



Citation: Zhang, H.; Hui, E.S.; Cao, P.; Mak, H.K.F. Relationship between Amyloid- β Deposition and the Coupling between Structural and Functional Brain Networks in Patients with Mild Cognitive Impairment and Alzheimer's Disease. *Brain Sci.* **2021**, *11*, 1535. <https://doi.org/10.3390/brainsci11111535>

Academic Editors: Omar Cauli, Pilar Pérez-Ros and Vanessa Ibáñez-del Valle

Received: 6 October 2021

Accepted: 17 November 2021

Published: 19 November 2021

Publisher's Note: MDPI stays neutral with regard to jurisdictional claims in published maps and institutional affiliations.



Copyright: © 2021 by the authors. Licensee MDPI, Basel, Switzerland. This article is an open access article distributed under the terms and conditions of the Creative Commons Attribution (CC BY) license (<https://creativecommons.org/licenses/by/4.0/>).

1. Introduction

Alzheimer's disease (AD), a chronic disease characterized by progressive memory loss and the deterioration of other cognitive functions, is one of the most common forms of dementia and results in death within 3 to 9 years after diagnosis [1]. Patients with AD are characterized by the progressive accumulation of two neuropathological hallmarks of AD, amyloid- β ($A\beta$) and tau [2], which eventually lead to the severe impairment of cognition and behavior.

Amyloid- β initially accumulates in the medial frontal and parietal cortices [3,4], while tau accumulates in the medial temporal lobe [5]. These pathological hallmarks of AD follow stage-dependent changes along the AD continuum [6]. It is of note that 82% of mild cognitive impairment (MCI) patients with Carbon-11 Pittsburgh compound B (¹¹C-PIB) retention, also known as $A\beta$ -positive, at baseline converted to AD at follow-up [7]; these patients (MCI_ $A\beta$ +) also converted to AD faster than MCI patients who were $A\beta$ -negative (MCI_ $A\beta$ -) [7–9].

Accumulation of A β has been shown to be associated with structural changes in subcortical volumes, cortical thickness, and surface area measures in healthy controls (HC) and MCI patients [10]. On the other hand, A β and tau pathologies also affect the anatomical and functional connections of the whole brain (known as structural and functional brain networks, respectively) in a stage-dependent manner [11]. It is of note that previous studies have focused on investigating the effect of AD pathologies on the structural or functional brain network alone. Considering these two types of brain connections are tightly coupled, whereby static anatomical connections facilitate and constrain the dynamic functional interactions between different brain regions [12–14], whether AD neuropathologies also exhibit stage-dependent effects on the interplay between these two types of brain connections warrants further investigation.

A potential approach to describe the interplay between the structural and functional brain networks is by the correlation between the two networks, known as structure-function (SC-FC) coupling [12–14]. The premise is that SC-FC coupling reflects the extent to which the structural brain network is constraining the functional brain network. The higher the coupling, the more the structural brain network constrains the functional brain network [15]. Recent studies have demonstrated that SC-FC coupling is decreased in patients with bipolar disorder [16], Parkinson's disease (PD) [17], multiple sclerosis (MS) [18], and AD [19]. The spatial variation in SC-FC coupling was found to be consistent with the functional specialization of the cortex; SC-FC coupling of the rostralateral prefrontal cortex was correlated with executive function in young adults [15].

The central hypothesis of this study is that SC-FC coupling is a novel biomarker for the characterization of the effect of A β accumulation along the AD continuum. We have previously shown that the majority of MCI patients can be distinguished from AD patients based on ¹⁸F-flutemetamol PET-CT scans with high efficacy [20]. Those who could not be differentiated were the MCI_A β + patients who had similar A β retention as AD patients. In this study, we therefore aim to investigate whether the effect of A β pathology on the global coupling between structural and functional brain networks would differ along the AD continuum, as defined by A β retention on ¹⁸F-flutemetamol PET-CT scans.

2. Materials and Methods

2.1. Participants

Forty-seven patients older than 55 years-old were recruited from the memory clinic of a university hospital for an MRI and ¹⁸F-flutemetamol PET-CT scans between June 2017 and June 2019. Subjects with a history of stroke, head injury, seizures, migraine, cancer within five years, active infection, end-stage renal or other organ failures, non-ambulatory or psychiatric diseases, regular alcohol consumption, and drug abuse were excluded. Fourteen healthy adults were recruited from social centers. Inclusion criteria included normal blood pressure (less than 140/90 mmHg) and a normal Montreal Cognitive Assessment (MoCA) cognitive score (≥ 26).

Ethical approval from the Institutional Review Board of the University of Hong Kong and Hospital Authority Hong Kong West Cluster was obtained (IRB reference number: UW 11-126, 11 April 2015), and our study complied with the Declaration of Helsinki. Written informed consent was obtained from all non-demented participants and the next of kin or caregivers of demented subjects. All participants underwent clinical evaluation, neuropsychological testing, and MRI including structural MRI, resting state functional MRI (rs-fMRI), diffusion tensor imaging (DTI), and arterial spin labelling (ASL). Only patients with mild cognitive impairment (MCI) or Alzheimer's disease (AD) received magnetic resonance angiography (MRA) and ¹⁸F-flutemetamol PET-CT scans. The MRI and PET-CT scans were performed within one week of each other.

2.2. Clinical and Neuropsychological Assessment

All participants underwent clinical evaluation, performed by a research nurse, and the Hong Kong version of the Montreal Cognitive Assessment test (HK-MoCA) [21], performed by a trained research assistant.

2.3. MRI Acquisition

MRI scans were performed using a 3 Tesla MRI scanner (Achieva TX, Philips, The Netherlands) with a standard 32-channel head coil. Structural images were acquired using 3D T1-weighted MPRAGE in the sagittal orientation with repetition time (TR)/echo time (TE)/inversion time = 6.8/3.2/847.9 ms, flip angle = 8°, field of view (FOV) = 256 × 240 × 204 mm³, and image resolution = 1 × 1 × 1.2 mm³. 3D FLAIR images were obtained with TR/TE = 4800/267 ms, thickness = 1.2 mm, FOV = 250 × 250 × 185 mm³, and image resolution = 1.2 × 1.2 × 1.12 mm³. DTI images were acquired with a spin-echo echo-planar sequence with TR/TE = 3900/81 ms, FOV = 230 × 230 mm², image resolution = 3 × 3.1 mm² (slice thickness of 3 mm), b-values of 0 and 1000 s/mm², and 15 diffusion gradient directions. rs-fMRI images were obtained with a gradient-echo echo-planar sequence with TR/TE = 2000/30 ms, flip angle = 90°, FOV = 230 × 230 × 144 (mm), image resolution = 3.28 × 3.28 mm², slice thickness = 4 mm, and number of volume = 180. During the rs-fMRI, participants were instructed to focus on a cross in the mirror and not think about anything.

2.4. PET-CT Acquisition

Patients with MCI or AD ($n = 47$) were required to fast for at least 6 h before the ¹⁸F-flutemetamol PET-CT scan. A bolus of ¹⁸F-flutemetamol at a dose of 185 MBq (nearly 5 mCi) was administered intravenously within 40 s. The scans were performed 90 min after the injection using an integrated in-line PET/CT scanner with 3D list mode. The duration of the scan was 30 min. Images were reconstructed using filtered back-projection with a slice thickness = 2~4 mm, matrix size = 128 × 128, and pixel size = 2 mm, with a full-width half-maximum (FWHM) post-smoothing filter with a Gaussian kernel of 5 mm.

2.5. White Matter Lesion Quantification

FLAIR images were used to quantify subcortical and periventricular white matter lesions using the Fazekas scale [22] by a trained scientist and were subsequently verified by an experienced neuroradiologist.

2.6. Dementia/Cognitively Impaired Subtype Classification

The diagnosis of cognitive impairment was determined by the consensus between a neuroradiologist (HKFM) and two geriatricians (YFS, PC, or JSKK) based on the findings from clinical (baseline and follow-up) and neuropsychological (HK-MoCA) evaluations, ¹⁸F-flutemetamol PET-CT scans, structural MRI, MRA, and ASL [20]. The diagnoses of MCI were determined using the clinical criteria from [23] and those of AD from [24] together with a positive A β diagnosis.

2.7. Amyloid Burden

The visual assessment of ¹⁸F-flutemetamol PET-CT scans was performed to determine whether an MCI patient was A β -positive or negative according to the criteria used in previous studies [25,26]. The assessment was performed by an experienced neuroradiologist (HKFM) who had successfully completed an electronic training program developed by GE Healthcare for the interpretation of ¹⁸F-Flutemetamol images.

The post-processing procedure included realignment, co-registration, and normalization using semi-automatic commercially available software (Cortex ID software, GE Healthcare Ltd., Waukesha, WI, USA). Quantitative analysis of 16 regions of interest (ROIs) was made by the Cortex ID software, including bilateral prefrontal, anterior cingulate, precuneus/posterior cingulate, parietal, lateral temporal, occipital, sensorimotor, and mesial

temporal regions. Standardized uptake values (SUVs) were calculated in all regions and normalized for the injected dose and body weight of each subject. The standardized uptake value ratio (SUVR) was defined as the ratio between two SUVs of different regions from within a single scan to avoid the bias of injected activity, using body weight and the volume to mass conversion factor, and was referenced to the pons in our data. The composite SUVR, representing the global A β burden, was calculated as the average SUVR value of the area-weighted mean for the 16 cortical ROIs. Cortex ID also offered regional z-scores as compared with a normal database for ^{18}F -flutemetamol.

2.8. Network Construction

2.8.1. Anatomical Parcellation

The entire brain was segmented into 90 regions (45 regions per hemisphere) using the automated anatomical labelling (AAL) template [27]. These regions were subsequently used as the nodes of the structural and functional connectivity networks for each subject.

2.8.2. Structural Brain Network Construction

The DTI data were corrected for motion and eddy current geometric distortions and brain tissue extraction was performed using the fMRIB Software Library, Oxford, UK' (FSL, <http://fsl.fmrib.ox.ac.uk/fsl>, accessed on 21 November 2020). Whole-brain tractography was conducted in the native space using the Fiber Assignment by Continuous Tracking algorithm from the Diffusion Toolkit (Athinoula A. Martinos Center for Biomedical Imaging, Massachusetts, MA, USA; <http://trackvis.org/dtk/>, accessed on 21 November 2020) with an FA threshold of 0.1 and an angle threshold of 35°. The brain parcellations from AAL in the standard Montreal Neurological Institute (MNI) space were warped to the individual's native space by the inverse transformations of image normalization and co-registration using SPM12 (The Wellcome Centre for Human Neuroimaging, London, UK; <https://www.fil.ion.ucl.ac.uk/spm/software/spm12/>, accessed on 9 January 2020). The fiber number between different brain parcellations was obtained using the UCLA Multimodal Connectivity Package (Center for Cognitive Neuroscience, University of California, Los Angeles, CA, USA; <https://www.ccn.ucla.edu/wiki/index.php>, accessed on 8 December 2020). A 90 \times 90 structural connectivity (SC) matrix was obtained for subsequent analyses.

2.8.3. Functional Brain Network Construction

The analysis of the rs-fMRI data was performed using the DPABI toolbox (State Key Laboratory of Cognitive Neuroscience and Learning & IDG/McGovern Institute for Brain Research, Beijing Normal University, Beijing, China; <http://rfmri.org/dpabi>, accessed on 9 January 2020) based on SPM12. The first ten dynamics were discarded, and the slices were corrected for different signal acquisition times. Next, the rs-fMRI data were realigned using a six-parameter (rigid body) linear transformation with a two-pass procedure (registered to the first volume and then registered to the mean of all volumes after the first realignment). Subjects with head movements more than 3 mm in any direction or over 3° were excluded in subsequent analysis. Tissue maps were obtained from T1 structural images. The Diffeomorphic Anatomical Registration Through Exponentiated Lie algebra (DARTEL) tool [28] was used to normalize the structural images and tissue maps to the MNI space. Several nuisance signals, including Friston 24 head motion parameters [29] derived from realignment, and mean white matter and cerebrospinal fluid time series were regressed out from the time course in each voxel. All fMRI images were spatially normalized to the MNI space and resampled to 3 \times 3 \times 3 mm³ using the transformation parameters from DARTEL. The rs-fMRI data were then band-pass filtered (0.01 < frequency < 0.1 Hz) to reduce high-frequency components from respiratory and cardiac motion and low-frequency drift. Linear trends were also removed. Brain regional time series was subsequently obtained by averaging the rs-fMRI signal of the voxels of each brain parcellation from AAL. The 90 \times 90 functional connectivity (FC) matrix was

subsequently obtained by correlation between the time series of all pairs of brain regions. Fisher z-transformation was applied to transform the correlation coefficients. FC matrix entry with a negative correlation coefficient was set as zero [30].

2.9. The Structural–Functional Connectivity Coupling

To estimate the coupling between the structural and functional brain networks, the following procedures were performed: (1) brain connections without any structural connections were discarded; (2) the distribution of structural connections was rescaled to a Gaussian distribution [12]; and (3) Pearson correlation was performed between the entire SC and FC matrices. The resulting correlation coefficient was regarded as the coupling of the two networks, denoted as SC-FC coupling from hereon.

2.10. Statistical Analysis

All statistical analyses were performed using SPSS (SPSS Inc., Chicago, IL, USA). Brown–Forsythe ANOVA with Tukey’s post hoc test was performed for group statistics. Sex was tested using Pearson’s Chi-square test. The relationships between A β deposition and SC-FC coupling and between A β deposition and MoCA scores were estimated using partial Pearson correlation with age, sex, and Fazekas score as covariates. The correlation was performed separately for the cognitively impaired subjects with positive and negative A β deposition. A significance level of $p < 0.05$ was set for all statistical tests.

3. Results

A total of 61 subjects, including 47 patients (MCI_A β -: $n = 21$; MCI_A β +: $n = 12$; AD: $n = 14$) and 14 controls, were recruited. Two controls, one MCI_A β +, and two AD patients were excluded due to head motion during the rs-fMRI and DTI scans. The demographic and clinical characteristics of these subjects are summarized in Table 1. HC were significantly younger ($p < 0.001$; age: 54 ± 16.8 years old) than the patient cohorts. MCI_A β - (MoCA: 23.0 ± 3.2 ; Fazekas scale: 3.95 ± 1.28), MCI_A β + (MoCA: 19.0 ± 4.3 ; Fazekas scale: 3.64 ± 1.80), and AD (MoCA: 12.0 ± 7.6 ; Fazekas scale: 3.00 ± 1.65) patients had significantly ($p < 0.001$) lower MoCA and higher Fazekas scores than HC (MoCA: 28.7 ± 1.3 ; Fazekas scale: 0.58 ± 0.67), with MCI_A β - patients having significantly ($p = 0.004$) higher MoCA scores than AD patients. MCI_A β + (0.71 ± 0.12) and AD (0.78 ± 0.10) patients had a significantly ($p < 0.001$) higher A β deposition when compared with MCI_A β - (0.42 ± 0.04) patients.

Table 1. Demographic and clinical characteristics of healthy controls and patients with mild cognitive impairment or Alzheimer’s disease.

	HC	MCI_A β -	MCI_A β +	AD	<i>p</i> -Value
Final sample size (n) [^]	12	21	11	12	-
Age range	54.0 ± 16.8 ^{a,b,c}	75.9 ± 7.0 ^a	74.5 ± 7.6 ^b	74.5 ± 8.7 ^c	<0.001
Sex (female/male)	7/5	11/10	7/4	7/5	0.94
HK-MoCA	28.7 ± 1.3 ^{d,e,f} ($n = 12$)	23.0 ± 3.2 ^{d,g} ($n = 19$)	19.0 ± 4.3 ^e ($n = 7$)	12.0 ± 7.6 ^{f,g} ($n = 9$)	<0.001
Fazekas Scale	0.58 ± 0.67 ^{h,i,j}	3.95 ± 1.28 ^h	3.64 ± 1.80 ⁱ	3.00 ± 1.65 ^j	<0.001
A β deposition	-	0.42 ± 0.04 ^{k,l}	0.71 ± 0.12 ^k	0.78 ± 0.10 ^l	<0.001
Global SC-FC coupling	0.13 ± 0.04	0.20 ± 0.03	0.26 ± 0.04	0.16 ± 0.04	0.16

Brown–Forsythe ANOVA with post hoc test: ^{c,g,j} $p < 0.05$; ^{a,b,d,e,f,h,i,k,l} $p < 0.01$ [^] after excluding subjects with large head motions. HC: healthy controls; A β : amyloid beta; MCI_A β -: mild cognitive impairment patient with negative A β ; MCI_A β +: mild cognitive impairment patient with positive A β ; AD: Alzheimer’s disease; SC-FC: structural-functional connectivity.

Figure 1 shows the group average of ¹⁸F-flutemetamol PET-CT images from the MCI_A β -, MCI_A β +, and AD cohorts.

After controlling for age, sex, and Fazekas score, a significant negative correlation ($r = -0.634$, $p < 0.001$) between MoCA scores and whole-brain A β deposition was observed (Figure 2).

Table 1 and Figure 3 illustrate the SC-FC coupling of different patient cohorts.

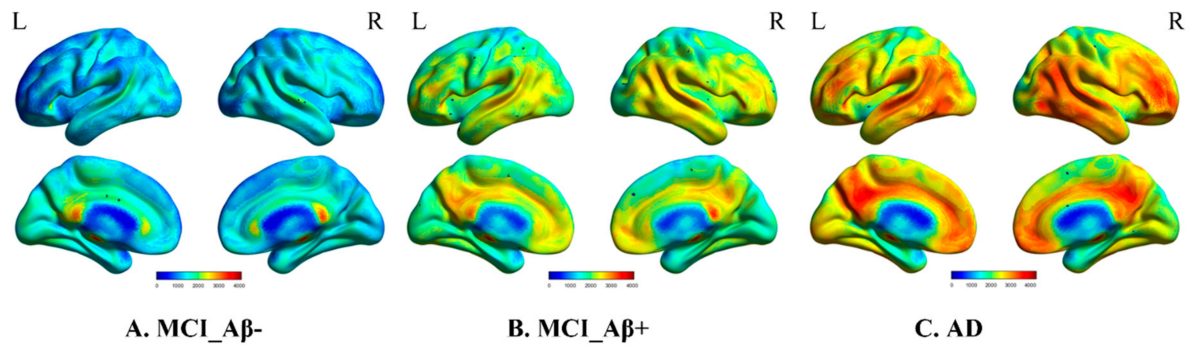


Figure 1. ¹⁸F-flutemetamol PET-CT images of patients with (A) MCI_{Aβ-}, (B) MCI_{Aβ+}, and (C) AD. HC: healthy controls; Aβ: amyloid beta; MCI_{Aβ-}: mild cognitive impairment patient with negative Aβ; MCI_{Aβ+}: mild cognitive impairment patient with positive Aβ; AD: Alzheimer's disease.

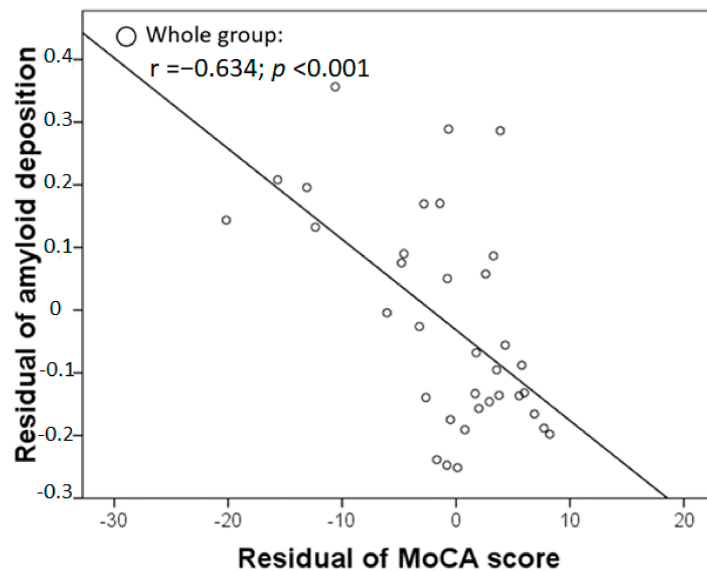


Figure 2. Scatter plot between MoCA score and the whole-brain Aβ deposition (partial Pearson correlation controlling for age, sex and Fazekas score). Aβ: amyloid beta; MoCA: Montreal Cognitive Assessment.

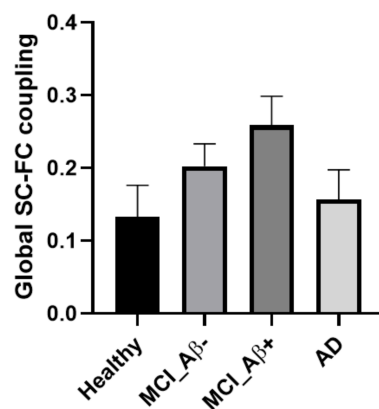


Figure 3. Group comparison of global coupling between structural and functional brain networks (SC-FC coupling) for different cohorts. Note that there was no significant difference between groups (p -value = 0.16; one-way Brown–Forsythe ANOVA).

There was no significant difference in global SC-FC coupling between groups ($p = 0.16$); however, an increasing trend in HC to MCI_A β + patients was observed. After adjusting for age, sex, and Fazekas score, there was a significant negative correlation between A β deposition and the SC-FC coupling ($r = -0.719$, $p = 0.044$; Figure 4B) for MCI_A β + patients, and a significant positive correlation for AD patients ($r = 0.700$, $p = 0.036$; Figure 4C), but no significant correlation for MCI_A β - patients ($r = 0.032$, $p = 0.899$, Figure 4A).

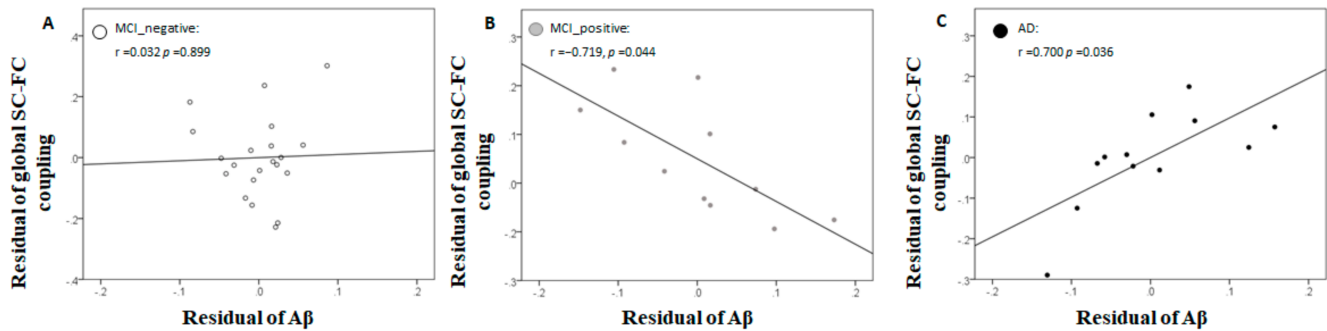


Figure 4. Scatter plots between A β deposition and global SC-FC coupling after controlling for age, sex, and Fazekas score for (A) MCI_A β -, (B) MCI_A β +, and (C) AD patients. Partial Pearson correlation controlling for age, sex, and Fazekas score was performed.

4. Discussion

The effect of amyloid- β along the Alzheimer's disease continuum was investigated using the global coupling between structural and functional brain networks. Although there was no difference in group-level global SC-FC coupling between different patient cohorts, A β pathology had distinctive stage-specific effects on the global coupling, consistent with previous studies that have investigated the structural and functional brain networks of AD separately [11].

4.1. Prodromal Alzheimer's Disease

Our results show that, during the prodromal stage of AD, the effect of A β pathology on global SC-FC coupling was markedly different in that significant negative association was only observed for MCI_A β + patients (Figure 4B) but not MCI_A β - patients (Figure 4A). These results may indicate that the global coupling between the structural and functional brain networks of MCI_A β - patients could be resilient to A β pathology during the early phase of A β accumulation. This may be attributable to the relatively focal effect of A β , as it initially preferentially accumulates only in a few selected locations of the brain, primarily the default mode network [4].

When the A β level became abnormal, the global SC-FC coupling of MCI_A β + patients decreased with the level of A β pathology (Figure 4B) and showed an increasing group-level trend compared to HC (Figure 3). Previous studies have demonstrated that abnormality in functional connectivity during this phase of AD progression was correlated with the levels of A β pathology, but not tau pathology, in preclinical and prodromal AD [31,32]; this association first occurred in the default mode network in preclinical AD, before gradually spreading to other brain networks over the AD continuum [33]. Apart from the functional brain network, the association between the topology of the structural brain network and the A β burden for patients with MCI [34] along with a diffuse loss of structural connectivity over the course of A β accumulation was also observed [35,36]. Taken together, the progressive effect of A β pathology up to the prodromal stage of AD not only affects structural and functional brain networks individually, but also the global coupling between the two networks.

It is of note that the global coupling of MCI_A β + patients decreased as the A β burden increased amidst an increasing group-level trend compared to HC. According to a study of regional SC-FC coupling by Gu et al., lower-order brain regions, such as those in the

visual and subcortical networks, tend to have higher regional coupling, likely suggesting that the direct structural connections underlying these brain regions serve as the main relay for propagation of brain signals [37]. On the other hand, the higher-order cortices, such as those in the default mode network, tend to have lower regional coupling, likely suggesting that the indirect structural connections underlying these cortical areas may be more important for signal relay [37]. Taken together, the negative association between the A β pathology and global SC-FC coupling of MCI_A β + patients may indicate that the direct structural connections between different regions across the brain gradually cannot constrain and facilitate the underlying brain signal propagation as A β burden increases.

4.2. Alzheimer's Disease Dementia

Our results show a contrasting effect of A β pathology on the global SC-FC coupling of patients with MCI_A β + (Figure 4B) versus those with AD (Figure 4C), despite their similar level of A β burden. Previous studies have shown that A β accumulation diffusely spreads across the cerebral cortex in the transition from prodromal AD to AD [38,39]. More importantly, the functional connectivity of the hub of multiple functional brain networks was shown to be associated with A β pathology [40], and that A β accumulation was colocalized with these abnormal functional connectivities for patients with AD [41]. Taken together, the fact that the effect of A β pathology spreads from non-hub brain regions to hub regions in the functional brain network during the AD dementia stage may underpin the contrasting effect on global SC-FC coupling observed in patients with MCI_A β + versus those with AD. Of note is that the interpretation of our results may be confounded by the interactive effects of A β and tau on functional connectivity [42].

4.3. Previous Investigations of Brain Network Coupling in Alzheimer's Disease

In a study of 38 normal controls, 40 MCI patients, and 19 AD patients, the SC-FC coupling of all connections of MCI and AD patients was enhanced, but no difference was found in the rich club connections compared to normal controls [43]. Another study on patients with mild cognitive impairment with no dementia (CIND, similar to MCI; $n = 61$) and moderate CIND ($n = 56$) demonstrated that moderate CIND patients showed higher global SC-FC coupling than healthy older subjects [44]. Another study showed no significant difference in global SC-FC coupling between AD patients and healthy controls, as well as the increased coupling of the default mode network of AD patients [45]. On the contrary, Sun et al. reported a significant decrease in the global SC-FC coupling of AD patients ($n = 12$) compared to HC ($n = 14$) and amnesic MCI patients ($n = 15$) [18]. Together with the results of our study showing no significant group difference in global SC-FC coupling, the inconsistency in these findings may be the result of the variations in the methods used for brain network construction and diagnostic criteria of MCI and AD.

4.4. Limitations

Firstly, because tau is another hallmark pathology of AD [42,46], its effect on the SC-FC coupling warrants further investigation. In particular, tau accumulation was demonstrated to be associated with functional connectivity regardless of the presence of A β deposition and dementia symptoms [47]. The investigation of the effect of tau on global coupling may thus potentially provide new knowledge on how to disentangle the contrasting effect of A β on the global coupling of patients with MCI_A β + versus those with AD. Secondly, previous studies have demonstrated that several factors, such as genes, age, and cognitive reserve (CR), could modify the progression from prodromal AD to AD [6]. In particular, CR could influence the trajectory of AD progression [48]. It would therefore be worthwhile to investigate whether the association between A β pathology and global coupling along the AD continuum would change for patients with high CR versus those with low CR. Thirdly, our DTI data were acquired along 15 diffusion-encoding directions to reduce the total scan time, thereby increasing the bias in the estimation of white matter tracts.

5. Conclusions

We successfully demonstrated that A β pathology has distinctive stage-specific effects on the global coupling between the structural and functional brain networks.

Author Contributions: Conceptualization, E.S.H. and H.K.F.M.; Formal analysis, H.Z.; Funding acquisition, H.K.F.M.; Investigation, E.S.H., P.C. and H.K.F.M.; Methodology, H.Z., E.S.H., H.Z. and P.C.; Project administration, H.K.F.M.; Supervision, E.S.H. and H.K.F.M.; Validation, E.S.H. and H.K.F.M.; Visualization, H.Z. and E.S.H.; Writing—original draft, H.Z. and H.K.F.M.; Writing—review and editing, E.S.H. and H.K.F.M. All authors have read and agreed to the published version of the manuscript.

Funding: This work was supported by the State Key Laboratory of Brain and Cognitive Sciences, the University of Hong Kong.

Institutional Review Board Statement: This study was approved by the institutional review board (IRB) of the University of Hong Kong/ Hospital Authority Hong Kong West Cluster (IRB reference number: UW 11-126, 11 April 2015). Written informed consent forms were obtained.

Informed Consent Statement: Informed consent was obtained from all subjects involved in the study.

Data Availability Statement: The data presented in this study are available on request from the corresponding author.

Conflicts of Interest: The authors declare no conflict of interest. The funders had no role in the design of the study; in the collection, analysis, or interpretation of data; in the writing of the manuscript; or in the decision to publish the results.

References

1. Querfurth, H.W.; LaFerla, F.M. Alzheimer's disease. *N. Engl. J. Med.* **2010**, *362*, 329–344. [[CrossRef](#)] [[PubMed](#)]
2. Hardy, J.A.; Higgins, G.A. Alzheimer's disease: The amyloid cascade hypothesis. *Science* **1992**, *256*, 184–185. [[CrossRef](#)] [[PubMed](#)]
3. Sperling, R.A.; Laviolette, P.S.; O'Keefe, K.; O'Brien, J.; Rentz, D.M.; Pihlajamaki, M.; Marshall, G.; Hyman, B.T.; Selkoe, D.J.; Hedden, T.; et al. Amyloid deposition is associated with impaired default network function in older persons without dementia. *Neuron* **2009**, *63*, 178–188. [[CrossRef](#)] [[PubMed](#)]
4. Palmqvist, S.; Scholl, M.; Strandberg, O.; Mattsson, N.; Stomrud, E.; Zetterberg, H.; Blennow, K.; Landau, S.; Jagust, W.; Hansson, O. Earliest accumulation of beta-amyloid occurs within the default-mode network and concurrently affects brain connectivity. *Nat. Commun.* **2017**, *8*, 1214. [[CrossRef](#)]
5. Small, S.A.; Schobel, S.A.; Buxton, R.B.; Witter, M.P.; Barnes, C.A. A pathophysiological framework of hippocampal dysfunction in ageing and disease. *Nat. Rev. Neurosci.* **2011**, *12*, 585–601. [[CrossRef](#)]
6. Jack, C.R.; Knopman, D.S.; Jagust, W.J.; Petersen, R.C.; Weiner, M.W.; Aisen, P.S.; Shaw, L.M.; Vemuri, P.; Wiste, H.J.; Weigand, S.D.; et al. Tracking pathophysiological processes in Alzheimer's disease: An updated hypothetical model of dynamic biomarkers. *Lancet Neurol.* **2013**, *12*, 207–216. [[CrossRef](#)]
7. Okello, A.; Koivunen, J.; Edison, P.; Archer, H.A.; Turkheimer, F.E.; Nagren, K.; Bullock, R.; Walker, Z.; Kennedy, A.; Fox, N.C.; et al. Conversion of amyloid positive and negative MCI to AD over 3 years: An 11C-PIB PET study. *Neurology* **2009**, *73*, 754–760. [[CrossRef](#)]
8. Forsberg, A.; Engler, H.; Almkvist, O.; Blomquist, G.; Hagman, G.; Wall, A.; Ringheim, A.; Langstrom, B.; Nordberg, A. PET imaging of amyloid deposition in patients with mild cognitive impairment. *Neurobiol. Aging* **2008**, *29*, 1456–1465. [[CrossRef](#)]
9. Roberts, R.O.; Aakre, J.A.; Kremers, W.K.; Vassilaki, M.; Knopman, D.S.; Mielke, M.M.; Alhurani, R.; Geda, Y.E.; Machulda, M.M.; Coloma, P.; et al. Prevalence and Outcomes of Amyloid Positivity Among Persons without Dementia in a Longitudinal, Population-Based Setting. *JAMA Neurol.* **2018**, *75*, 970–979. [[CrossRef](#)]
10. Ten Kate, M.; Redolfi, A.; Peira, E.; Bos, I.; Vos, S.J.; Vandenberghe, R.; Gabel, S.; Schaeferbeke, J.; Scheltens, P.; Blin, O.; et al. MRI predictors of amyloid pathology: Results from the EMIF-AD Multimodal Biomarker Discovery study. *Alzheimer's Res. Ther.* **2018**, *10*, 100. [[CrossRef](#)]
11. Yu, M.; Sporns, O.; Saykin, A.J. The human connectome in Alzheimer disease—relationship to biomarkers and genetics. *Nat. Rev. Neurosci.* **2021**, *17*, 545–563. [[CrossRef](#)]
12. Honey, C.J.; Sporns, O.; Cammoun, L.; Gigandet, X.; Thiran, J.P.; Meuli, R.; Hagmann, P. Predicting human resting-state functional connectivity from structural connectivity. *Proc. Natl. Acad. Sci. USA* **2009**, *106*, 2035–2040. [[CrossRef](#)]
13. Honey, C.J.; Thivierge, J.P.; Sporns, O. Can structure predict function in the human brain? *Neuroimage* **2010**, *52*, 766–776. [[CrossRef](#)]
14. Zhang, Z.; Liao, W.; Chen, H.; Mantini, D.; Ding, J.R.; Xu, Q.; Wang, Z.; Yuan, C.; Chen, G.; Jiao, Q.; et al. Altered functional-structural coupling of large-scale brain networks in idiopathic generalized epilepsy. *Brain* **2011**, *134*, 2912–2928. [[CrossRef](#)]
15. Baum, G.L.; Cui, Z.; Roalf, D.R.; Ciric, R.; Betzel, R.F.; Larsen, B.; Cieslak, M.; Cook, P.A.; Xia, C.H.; Moore, T.M.; et al. Development of structure-function coupling in human brain networks during youth. *Proc. Natl. Acad. Sci. USA* **2020**, *117*, 771–778. [[CrossRef](#)]

16. Zhang, R.; Shao, R.; Xu, G.; Lu, W.; Zheng, W.; Miao, Q.; Chen, K.; Gao, Y.; Bi, Y.; Guan, L.; et al. Aberrant brain structural-functional connectivity coupling in euthymic bipolar disorder. *Hum. Brain Mapp.* **2019**, *40*, 3452–3463. [[CrossRef](#)]
17. Zarkali, A.; McColgan, P.; Leyland, L.A.; Lees, A.J.; Rees, G.; Weil, R.S. Organisational and neuromodulatory underpinnings of structural-functional connectivity decoupling in patients with Parkinson's disease. *Commun. Biol.* **2021**, *4*, 86. [[CrossRef](#)]
18. Koubiyr, I.; Besson, P.; Deloire, M.; Charre-Morin, J.; Saubusse, A.; Tourdias, T.; Brochet, B.; Ruet, A. Dynamic modular-level alterations of structural-functional coupling in clinically isolated syndrome. *Brain* **2019**, *142*, 3428–3439. [[CrossRef](#)]
19. Sun, Y.; Yin, Q.; Fang, R.; Yan, X.; Wang, Y.; Bezerianos, A.; Tang, H.; Miao, F.; Sun, J. Disrupted functional brain connectivity and its association to structural connectivity in amnesic mild cognitive impairment and Alzheimer's disease. *PLoS ONE* **2014**, *9*, e96505. [[CrossRef](#)]
20. Bao, Y.W.; Chau, A.C.M.; Chiu, P.K.; Shea, Y.F.; Kwan, J.S.K.; Chan, F.H.W.; Mak, H.K. Heterogeneity of Amyloid Binding in Cognitively Impaired Patients Consecutively Recruited from a Memory Clinic: Evaluating the Utility of Quantitative 18F-Flutemetamol PET-CT in Discrimination of Mild Cognitive Impairment from Alzheimer's Disease and Other Dementias. *J. Alzheimer's Dis.* **2021**, *79*, 819–832. [[CrossRef](#)]
21. Wong, A.; Xiong, Y.Y.; Kwan, P.W.; Chan, A.Y.; Lam, W.W.; Wang, K.; Chu, W.C.; Nyenhuis, D.L.; Nasreddine, Z.; Wong, L.K.; et al. The validity, reliability and clinical utility of the Hong Kong Montreal Cognitive Assessment (HK-MoCA) in patients with cerebral small vessel disease. *Dement. Geriatr. Cogn. Disord.* **2009**, *28*, 81–87. [[CrossRef](#)]
22. Fazekas, F.; Chawluk, J.B.; Alavi, A.; Hurtig, H.I.; Zimmerman, R.A. MR signal abnormalities at 1.5 T in Alzheimer's dementia and normal aging. *AJR Am. J. Roentgenol.* **1987**, *149*, 351–356. [[CrossRef](#)]
23. Petersen, R.C.; Smith, G.E.; Waring, S.C.; Ivnik, R.J.; Tangalos, E.G.; Kokmen, E. Mild cognitive impairment: Clinical characterization and outcome. *Arch. Neurol.* **1999**, *56*, 303–308. [[CrossRef](#)]
24. McKhann, G.M.; Knopman, D.S.; Chertkow, H.; Hyman, B.T.; Jack, C.R., Jr.; Kawas, C.H.; Klunk, W.E.; Koroshetz, W.J.; Manly, J.J.; Mayeux, R.; et al. The diagnosis of dementia due to Alzheimer's disease: Recommendations from the National Institute on Aging-Alzheimer's Association workgroups on diagnostic guidelines for Alzheimer's disease. *Alzheimer's Dement.* **2011**, *7*, 263–269. [[CrossRef](#)]
25. Vandenberghe, R.; Van Laere, K.; Ivanou, A.; Salmon, E.; Bastin, C.; Triau, E.; Hasselbalch, S.; Law, I.; Andersen, A.; Korner, A.; et al. 18F-flutemetamol amyloid imaging in Alzheimer disease and mild cognitive impairment: A phase 2 trial. *Ann. Neurol.* **2010**, *68*, 319–329. [[CrossRef](#)]
26. Buckley, C.J.; Sherwin, P.F.; Smith, A.P.; Wolber, J.; Weick, S.M.; Brooks, D.J. Validation of an electronic image reader training programme for interpretation of [18F]flutemetamol beta-amyloid PET brain images. *Nucl. Med. Commun.* **2017**, *38*, 234–241. [[CrossRef](#)]
27. Tzourio-Mazoyer, N.; Landeau, B.; Papathanassiou, D.; Crivello, F.; Etard, O.; Delcroix, N.; Mazoyer, B.; Joliot, M. Automated anatomical labeling of activations in SPM using a macroscopic anatomical parcellation of the MNI MRI single-subject brain. *Neuroimage* **2002**, *15*, 273–289. [[CrossRef](#)]
28. Ashburner, J. A fast diffeomorphic image registration algorithm. *Neuroimage* **2007**, *38*, 95–113. [[CrossRef](#)]
29. Friston, K.J.; Williams, S.; Howard, R.; Frackowiak, R.S.; Turner, R. Movement-related effects in fMRI time-series. *Magn. Reson. Med.* **1996**, *35*, 346–355. [[CrossRef](#)]
30. Fox, M.D.; Zhang, D.; Snyder, A.Z.; Raichle, M.E. The global signal and observed anticorrelated resting state brain networks. *J. Neurophysiol.* **2009**, *101*, 3270–3283. [[CrossRef](#)]
31. Zuo, X.N.; Ehmke, R.; Mennes, M.; Imperati, D.; Castellanos, F.X.; Sporns, O.; Milham, M.P. Network centrality in the human functional connectome. *Cereb. Cortex* **2012**, *22*, 1862–1875. [[CrossRef](#)] [[PubMed](#)]
32. Millar, P.R.; Ances, B.M.; Gordon, B.A.; Benzinger, T.L.S.; Fagan, A.M.; Morris, J.C.; Balota, D.A. Evaluating resting-state BOLD variability in relation to biomarkers of preclinical Alzheimer's disease. *Neurobiol. Aging* **2020**, *96*, 233–245. [[CrossRef](#)] [[PubMed](#)]
33. Jones, D.T.; Knopman, D.S.; Gunter, J.L.; Graff-Radford, J.; Vemuri, P.; Boeve, B.F.; Petersen, R.C.; Weiner, M.W.; Jack, C.R., Jr.; Alzheimer's Disease Neuroimaging Initiative. Cascading network failure across the Alzheimer's disease spectrum. *Brain* **2016**, *139*, 547–562. [[CrossRef](#)] [[PubMed](#)]
34. Alexander-Bloch, A.; Giedd, J.N.; Bullmore, E. Imaging structural co-variance between human brain regions. *Nat. Rev. Neurosci.* **2013**, *14*, 322–336. [[CrossRef](#)]
35. Voevodskaya, O.; Pereira, J.B.; Volpe, G.; Lindberg, O.; Stomrud, E.; van Westen, D.; Westman, E.; Hansson, O. Altered structural network organization in cognitively normal individuals with amyloid pathology. *Neurobiol. Aging* **2018**, *64*, 15–24. [[CrossRef](#)]
36. Prescott, J.W.; Guidon, A.; Doraiswamy, P.M.; Roy Choudhury, K.; Liu, C.; Petrella, J.R.; Alzheimer's Disease Neuroimaging Initiative. The Alzheimer structural connectome: Changes in cortical network topology with increased amyloid plaque burden. *Radiology* **2014**, *273*, 175–184. [[CrossRef](#)]
37. Gu, Z.; Jamison, K.W.; Sabuncu, M.R.; Kuceyeski, A. Heritability and interindividual variability of regional structure-function coupling. *Nat. Commun.* **2021**, *12*, 4894. [[CrossRef](#)]
38. Gordon, B.A.; Blazey, T.M.; Su, Y.; Hari-Raj, A.; Dincer, A.; Flores, S.; Christensen, J.; McDade, E.; Wang, G.; Xiong, C.; et al. Spatial patterns of neuroimaging biomarker change in individuals from families with autosomal dominant Alzheimer's disease: A longitudinal study. *Lancet Neurol.* **2018**, *17*, 241–250. [[CrossRef](#)]

39. Benzinger, T.L.; Blazey, T.; Jack, C.R., Jr.; Koeppe, R.A.; Su, Y.; Xiong, C.; Raichle, M.E.; Snyder, A.Z.; Ances, B.M.; Bateman, R.J.; et al. Regional variability of imaging biomarkers in autosomal dominant Alzheimer's disease. *Proc. Natl. Acad. Sci. USA* **2013**, *110*, E4502–E4509. [[CrossRef](#)]
40. Yu, M.; Engels, M.M.A.; Hillebrand, A.; van Straaten, E.C.W.; Gouw, A.A.; Teunissen, C.; van der Flier, W.M.; Scheltens, P.; Stam, C.J. Selective impairment of hippocampus and posterior hub areas in Alzheimer's disease: An MEG-based multiplex network study. *Brain* **2017**, *140*, 1466–1485. [[CrossRef](#)]
41. Buckner, R.L.; Sepulcre, J.; Talukdar, T.; Krienen, F.M.; Liu, H.; Hedden, T.; Andrews-Hanna, J.R.; Sperling, R.A.; Johnson, K.A. Cortical hubs revealed by intrinsic functional connectivity: Mapping, assessment of stability, and relation to Alzheimer's disease. *J. Neurosci.* **2009**, *29*, 1860–1873. [[CrossRef](#)]
42. Schultz, A.P.; Chhatwal, J.P.; Hedden, T.; Mormino, E.C.; Hanseeuw, B.J.; Sepulcre, J.; Huijbers, W.; LaPoint, M.; Buckley, R.F.; Johnson, K.A.; et al. Phases of Hyperconnectivity and Hypoconnectivity in the Default Mode and Salience Networks Track with Amyloid and Tau in Clinically Normal Individuals. *J. Neurosci.* **2017**, *37*, 4323–4331. [[CrossRef](#)]
43. Cao, R.; Wang, X.; Gao, Y.; Li, T.; Zhang, H.; Hussain, W.; Xie, Y.; Wang, J.; Wang, B.; Xiang, J. Abnormal Anatomical Rich-Club Organization and Structural-Functional Coupling in Mild Cognitive Impairment and Alzheimer's Disease. *Front. Neurol.* **2020**, *11*, 53. [[CrossRef](#)]
44. Wang, J.; Khosrowabadi, R.; Ng, K.K.; Hong, Z.; Chong, J.S.X.; Wang, Y.; Chen, C.Y.; Hilal, S.; Venketasubramanian, N.; Wong, T.Y.; et al. Alterations in Brain Network Topology and Structural-Functional Connectome Coupling Relate to Cognitive Impairment. *Front. Aging Neurosci.* **2018**, *10*, 404. [[CrossRef](#)]
45. Dai, Z.; Lin, Q.; Li, T.; Wang, X.; Yuan, H.; Yu, X.; He, Y.; Wang, H. Disrupted structural and functional brain networks in Alzheimer's disease. *Neurobiol. Aging* **2019**, *75*, 71–82. [[CrossRef](#)]
46. Huijbers, W.; Schultz, A.P.; Papp, K.V.; LaPoint, M.R.; Hanseeuw, B.; Chhatwal, J.P.; Hedden, T.; Johnson, K.A.; Sperling, R.A. Tau Accumulation in Clinically Normal Older Adults Is Associated with Hippocampal Hyperactivity. *J. Neurosci.* **2019**, *39*, 548–556. [[CrossRef](#)]
47. Franzmeier, N.; Rubinski, A.; Neitzel, J.; Kim, Y.; Damm, A.; Na, D.L.; Kim, H.J.; Lyoo, C.H.; Cho, H.; Finsterwalder, S.; et al. Functional connectivity associated with tau levels in ageing, Alzheimer's, and small vessel disease. *Brain* **2019**, *142*, 1093–1107. [[CrossRef](#)]
48. Hatashita, S.; Wakebe, D. Amyloid-beta Deposition and Long-Term Progression in Mild Cognitive Impairment due to Alzheimer's Disease Defined with Amyloid PET Imaging. *J. Alzheimer's Dis.* **2017**, *57*, 765–773. [[CrossRef](#)]